SCIENCE CHINA Materials ARTICLES

mater.scichina.com link.springer.com

Published online 22 May 2019 | https://doi.org/10.1007/s40843-019-9436-1
Sci China Mater 2020, 63(10): 1889–1897

SPECIAL TOPIC: Graphene Oxides towards Practical Applications

Wet-spinning assembly of nitrogen-doped graphene film for stable graphene-polyaniline supercapacitor electrodes with high mass loading

Xingyuan Chu, Tieqi Huang*, Yueqi Hu, Ruilin Dong, Jingyang Luo, Shengying Cai, Weiwei Gao, Zhen Xu and Chao Gao*

ABSTRACT **Graphene-polyaniline (GP) composites are promising electrode materials for supercapacitors but possessing unsatisfied stability, especially under high mass loading, due to the low ion transmission efficiency and serious pulverization effect. To address this issue, we propose a scalable method to achieve highly wettable GP electrodes, showing excellent stability. In addition, our results demonstrate that the performance of electrodes is nearly independent of the mass loading, indicating the great potential of such GP electrodes for practical devices. We attribute the remarkable performance of GP to the delicate precursor of nitrogen doped graphene film assembled by wet-spinning technology. This report provides a strategy to promote the ion penetrating efficiency across the electrodes and deter the pulverization effect, aiming at the practical GP supercapacitor electrodes of high mass loading.**

Keywords: supercapacitor, graphene, polyaniline, nitrogen doping, stability, mass loading

INTRODUCTION

Supercapacitors (SCs) are known for their high power density to satisfy the requirements of specific fields such as heavy-duty applications and electric vehicles (EVs) [1]. Carbon based materials, especially graphene based materials, arrest great attention due to their high conductivity, high specific surface area (SSA) and stability [2]. Unfortunately, graphene electrodes normally suffer from low capacitance (< 250 F g^{-1} in most literatures) [3], resulting in poor energy storage (<10 W h kg^{-1}) [4]. To explore the next generation of supercapacitor electrodes that exceed 10 W h kg^{-1}, researchers have introduced kinds of pseudocapacitive components to graphene [5]. Among all the pseudocapacitive materials, polyaniline (PANi) shows ultrahigh capacitance based on fast and reversible faradaic redox reactions and considerable conductivity in aqueous electrolytes, and the combination of graphene and PANi (GP) becomes a potential method to achieve high capacitance [6]. However, the low stability caused by pulverization problem limits the potential of GP composites. Moreover, the mass loading of electrodes was barely studied in detail, which retarded the practical applications of GP materials. Developing GP electrodes with long lifespan and considerable mass loading is still a big challenge.

Here, we demonstrate a facile scalable preparation of nitrogen-doped graphene induced GP electrodes with excellent hydrophilia, performing stable energy storage even under high mass loading. The precursor of nitrogen-doped graphene film (NGF) was successively prepared *via* wet-spinning and hydrothermal reaction in the solution of NH_4HCO_3. Afterwards, *in situ* growth of PANi on graphene sheets occurred, mainly due to the nitrogen atoms that initiated the polymerization. The PANi grafted NGF (PNGF) displayed an ultrawettable property, and thus good electrochemical performance (360 F g^{-1} at 1 A g^{-1}, 78% retention after 20,000 cycles). Furthermore, the mass loading of PNGF electrode had negligible influence on the performance, showing 340 F g^{-1} at 1 A g^{-1} and 73% retention (20,000 cycles) under the mass loading of 10.34 mg cm^{-2}. Accordingly, we attribute such a highlight stability to the well-designed nitrogen-doping

MOE Key Laboratory of Macromolecular Synthesis and Functionalization, Key Laboratory of Novel Adsorption and Separation Materials and Application Technology of Zhejiang Province, Department of Polymer Science and Engineering, Zhejiang University, Hangzhou 310027, China
* Corresponding authors (emails: woshihuangtieqi@163.com (Huang T); chaogao@zju.edu.cn (Gao C))

layered structure, which not only ameliorates the wettability but also improves the efficiency of ion transmission in the electrodes. This work may shed a light on the real supercapacitor applications of GP materials.

EXPERIMENTAL SECTION

Materials

All the reagents were of analytical grade and used as received. Graphene oxide (GO) with average lateral size of 10 μm was purchased from www.gaoxitech.com.

Preparation of NHC-GO hydrogel film and NGF

GO aqueous solution (15 mg mL^{-1}) was spun into a coagulation bath (NH_4HCO_3, 10 wt%) from a designed flattened nozzle. After 1 h, GO was crosslinked and became hydrogel film (NHC-GO).

The NHC-GO hydrogel film was transferred into a closed Teflon-lined autoclave full-filled with aqueous bath (NH_4HCO_3, 10 wt%) and heated at 180°C for a suitable time (2 h if no specific instructions). The obtained black NGF was washed with water and stayed under the pressure of 10 MPa overnight.

By utilizing nozzles with different sizes, NGF was fabricated with different thicknesses and thus different mass loadings.

Preparation of GO hydrogel film and graphene film (GF)

GO hydrogel film and GF were prepared in the same way as NHC-GO hydrogel film and NGF, except using $CaCl_2$ (3 wt%) as the coagulation bath and aqueous bath.

Preparation of PNGF and PANi-graphene film (PGF)

Aniline (0.0312 g) was dropped in a flask, which contained 5 mL ethanol and 15 mL 1 mol L^{-1} HCl, and stirred for half an hour before NGF were dipped in. After 1 h, 0.0504 g ammonium persulfate in 5 mL HCl was added to the flask dropwise. The reaction was kept at −10°C without stirring for 12 h. Then the films were washed with deionized water to obtain PNGF. Using GFs to replace NGFs, PGFs were prepared with the same protocol as the case of PNGFs.

By utilizing NGF with different mass loadings as the template to grow PANi, PNGF with different mass loadings can be obtained.

Characterization

Scanning electron microscopy (SEM) images were observed by Hitachi S-4800. Raman spectra were acquired using a Renishaw in Via-Reflex Raman microscopy at an excitation wavelength of 532 nm. X-ray diffraction (XRD) was conducted on Rigaku D/max-2500, using graphite monochromatized Cu Kα radiation. X-ray photoelectron spectroscopy (XPS) measurements were acquired by a PHI 5000C ESCA system (Physical Electronics) operated at 14.0 kV. Fourier transform infrared (FTIR) spectra were collected on a Bruker Vector-22 FTIR spectrometer (4,000–400 cm^{-1}). Electrochemical measurements were carried out in cells with two symmetrical electrodes, using a mixed cellulose esters membrane as the separator (pore size 0.22 μm), platinum foils as the current collector, and 1 mol L^{-1} H_2SO_4 as the electrolyte. Cyclic voltammetry (CV), galvanostatic charge-discharge (GCD) and electrochemical impedance spectroscopy (EIS) tests were carried out using an electrochemical workstation (CHI660e, CH Instruments, Inc.).

RESULTS AND DISSCUSSION

The fabrication of PNGF is illustrated in Fig. 1. Previously, Gao *et al.* [7–9] found the lyotropic liquid crystallinity of GO in water and specific organic solvents, and set up the wet-spinning technology. A particularly designed nozzle apparatus was utilized to inject the GO liquid crystal (LC) spinning dopes from the spinning channel into the coagulation bath containing NH_4HCO_3 to obtain cross-linked hydrogel films successively, namely NHC-GO hydrogel films (Fig. 1b). After hydrothermal treatment (which reduced NHC-GO hydrogel films to NGF) and *in situ* polymerization of PANi on the precursor of NGF, PNGF can be fabricated (Fig. 1a). The PNGF can be bended and relaxed in cycles without obvious break ledge, indicating its potential as a free-standing electrode (Fig. 1c).

SEM images of GF, PGF, NGF and PNGF are shown in Fig. 2a–f. NGF shows much more crumpled structure than GF due to the nitrogen doping procedures (Fig. 2a, c), revealing more efficient ion transmission pathways [10]. Based on the precursor of NGF, the PANi nanoparticles can be clearly observed both on the surface and between the interlayers of PNGF (Fig. 2d–f), indicating the successful growth of PANi in the entire film. Compared with PNGF, the PGF exhibits obscure nanoparticles between the interlayers (Fig. 2b), which may be due to the more restacking structures of the precursor GF to be penetrated by aniline monomers. According to the SEM images, the precursor of NGF is conducive to the growth of PANi on the graphene sheets.

Fig. 2g shows the Raman spectra of the GF, PGF, NGF, PNGF and pure PANi. All of the graphene-based films have two typical peaks at about 1,352 and 1,600 cm^{-1},

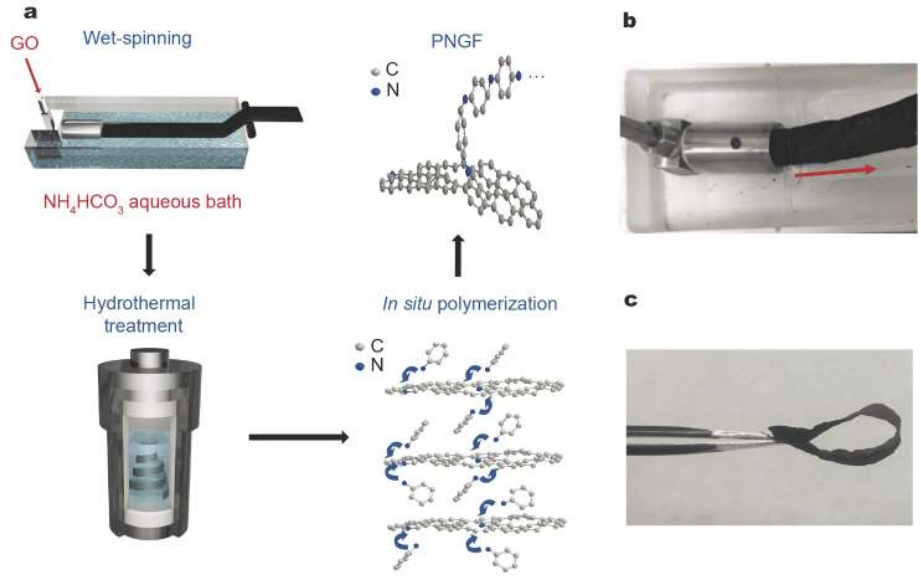

Figure 1 Fabrication procedure of PNGF. (a) Schematic of the scalable preparation of PNGF. (b) Photograph of wet-spinning step. (c) Optical image of PNGF at bending state.

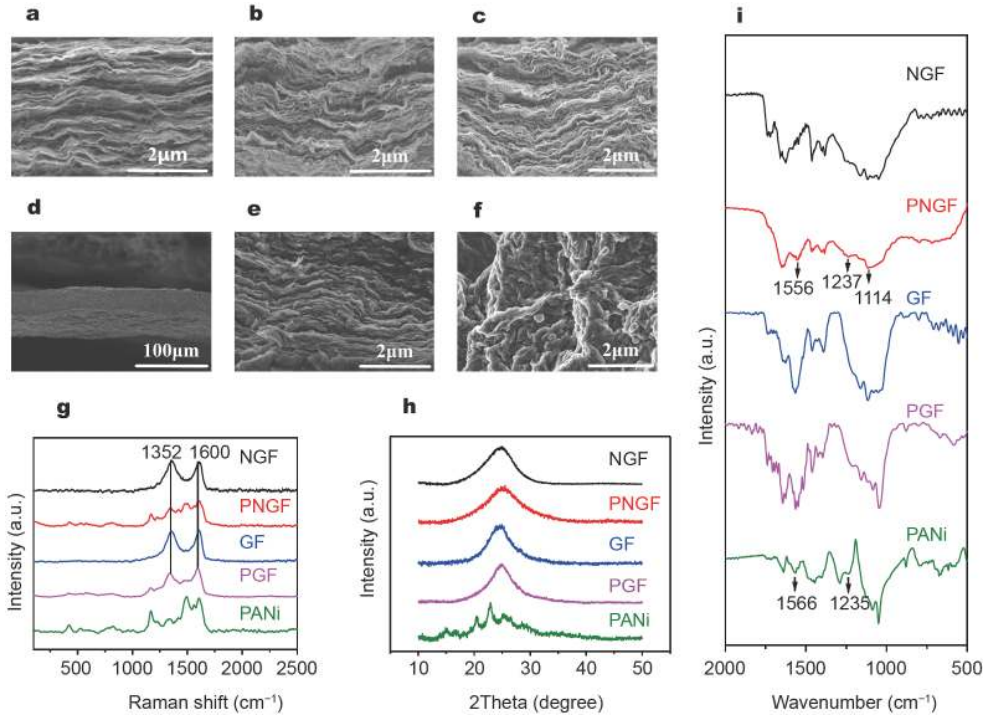

Figure 2 Characterization of NGF, PNGF, GF, PGF and PANi. Cross-section SEM images of GF (a), PGF (b), and NGF (c). (d, e) Cross-section SEM images of PNGF with different magnifications. (f) Top-view SEM image of the surface of PNGF. (g) Raman spectra of GF, PGF, NGF, PNGF and PANi. (h) XRD patterns of NGF, PNGF, GF, PGF and PANi. (i) FTIR spectra of NGF, PNGF, GF, PGF and PANi.

corresponding to the D-band and G-band, respectively [11]. The Raman spectrum of the PANi shows a series of characteristic peaks of PANi. The peaks at 1,168, 1,232, 1,341, 1,489 cm^{-1} are ascribed to the C–H bending deformation in the benzenoid ring, the C–N stretching vibration of the polaronic units, the semiquinone radical vibrations and the C=N stretching vibration of the quinonoid units, respectively [12]. All these peaks appear in

the spectrum of PNGF, confirming the successful doping of PANi on the precursor of the NGF. For comparison, there are only unconspicuous peaks in PGF at 1,164 and 1,510 cm^{-1}, which are assigned as the signal of PANi, demonstrating the poorish doping of PANi on the precursor of the GF [12]. This suggests that the precursors of graphene based materials affect the growth of PANi, and the grafting progress of PANi is easier to occur on NGF than GF.

The interlayer space of precursors was confirmed by XRD patterns. Fig. 2h shows the XRD patterns of the GF, PGF, NGF, PNGF and pure PANi with 2θ ranging from 10° to 50°. All of graphene-based films have a similar peak at around 25°, which can be correlated to the graphitic carbon (002) with an interlayer spacing of about 0.35 nm [13]. In detail, half-peak width of PNGF is obviously larger than that of NGF, indicating the low crystallization due to the generation of PANi between the graphene sheets [14]. However, the GF and PGF exhibit almost the same XRD patterns with narrow half-peak width, indicating inefficient destruction of graphene restacking structure for the polymerization of aniline. The results imply the importance of precursors again, as NGF exhibits higher activity than GF while grafting with PANi.

To further study the impacts of different precursors on the final GP materials, we utilized FTIR to analyze the combination mode of graphene based substrate and PANi (Fig. 2i). In the FTIR spectrum of PNGF, the peaks at 1,556 and 1,237 cm^{-1} are attributed to the C=C stretchings of quinonoid ring and C–H bendings of benzenoid ring, respectively. These characteristic peaks of PANi illustrate that this polymer grows on the precursor of NGF [12]. As for the precursor of GF, no new peaks from PANi arise after doping. It is worth mentioning that the peak at 1,114 cm^{-1} in the FTIR spectrum of PNGF may be attributed to the stretching of tertiary amine. Given that tertiary amine group is neither present in NGF nor PANi, we propose a possible chemical graft growth mechanism of PANi on the sheets of NGF (Fig. S1), rather than mere physical mixture of PANi with graphene based materials. The FTIR spectrum of physical mixture of PANi and GF shows no peaks attributing to tertiary amine, which also supports this point (Fig. S2). In addition, the nitrogen atoms on the sheets of NGF induce the successful binding with aniline, followed by *in-situ* polymerization.

The XPS spectra of the GF, PGF, NGF, PNGF and pure PANi are employed to illustrate the nitrogen composition (Fig. S3). The N 1s core-level XPS spectrum of the NGF is composed of three peaks, corresponding to three types of nitrogen functional groups, –NH– (399.9 eV), –N= (398.3 eV) and N^+ (400.9 eV) [10,15]. Similar to the previously reported nitrogen doped graphene materials, the –NH– type is dominant [16]. After doping, the peak of N^+ enhances and –N= disappears, implying the successful growth of PANi on the surface of the precursor of NGF [17]. However, both the GF and PGF have only one peak corresponding to –NH–, indicating that GF does not serve as good precursor for the growth of PANi as NGF, which is consistent with the aforementioned analysis. Moreover, the nitrogen content was confirmed by elemental analysis (EA) to reveal the different contents of PANi on such two different precursors (Table S1). Based on the calculated nitrogen contents between precursors and composite films, the mass fraction of PANi in the PNGF and PGF are 12.27% and 3.82%, respectively. It reveals that PANi is prior to combine with NGF than GF.

Considering the GP materials as electrodes of supercapacitors (SC), the interface of GP and electrolyte is quite important for the performance [18]. Fig. 3a presents the optical images of dynamic contact angle on GF, PGF, NGF, PNGF for the aqueous electrolyte of 1 mol L^{-1} H_2SO_4, which is estimated suitable for the pseudocapa-

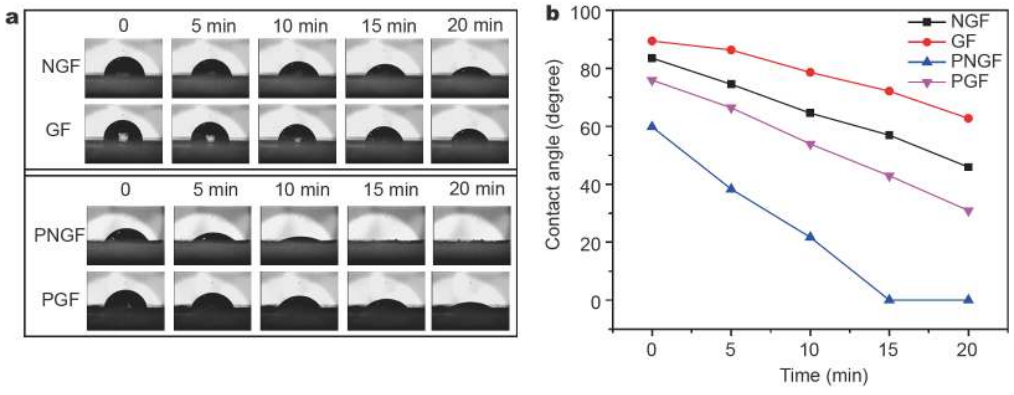

Figure 3 (a) Dynamic contact angle measurements for NGF, PNGF, GF and PGF. (b) The relationship between contact angle and contact time.

citance of PANi [13,19]. As shown in Fig. 3b, the relationship between contact angle and contact time demonstrates the wettability of NGF is better than that of GF, and that of PNGF is better than that of PGF, because NGF has numerous hydrophilic N atoms doped in the graphene [20]. Moreover, grafting of PANi significantly improves the wettability of NGF due to the hydrophilic N compositions (e.g., N^+), resulting in the contact angle decrease from 83.5° to 59.8°, which may further activate the connection between electrolyte ions and electrodes. On the other hand, although the doping of PANi does increase the wettability of GF (initially from 89.4° to 75.9°), the wettability of PGF still cannot be comparable with that of PNGF. Interestingly, the contact angle of PNGF turned into 0° after 15 min, whose wettability rate is 5.1° min^{-1}, demonstrating excellent wettability as a promising electrode for SCs. Notably, given the better affinity of nitrogen atoms than hydrophobic benzene rings with aqueous electrolyte, it can be estimated that the graft of aniline and its oligomer in aqueous solution is more efficient in NGF than in GF. This leads to larger content of PANi in PNGF than in PGF, consistent with the aforementioned EA results. As a result, the better wettability of NGF and PNGF facilitates the ion diffusion and increases the ion-accessible surface, which satisfies the general requirements for SC electrode materials [21].

The corresponding SCs utilizing GF, PGF, NGF and PNGF as free-standing electrodes are denoted as GF-SC, PGF-SC, NGF-SC and PNGF-SC. They were assembled into two-electrode system, as indicated by the practical assembly of real SCs [22]. Fig. 4a shows the CV curves of the GF-SC, PGF-SC, NGF-SC and PNGF-SC. GF-SC exhibits a semi-rectangular shape, indicating good electric double layer (EDL) capacitance properties [23], which shares a similar shape with the NGF-SC with higher integral area. A pair of intense peaks shown in both of PNGF-SC and PGF-SC is attributed to the redox reactions of PANi, corresponding to the emeraldine/pernigraniline structural conversions, respectively [24]. However, the CV curve of the PNGF-SC exhibits larger rectangular area than that of the PGF-SC, signifying larger pseudocapacitance.

To further quantify the gravimetric specific capacitance (C_g) of these electrodes, the GCD curves are shown in Fig. 4b. The GF-SC and NGF-SC exhibit good symmetrical linear curves at the current density of 1 A g^{-1}, implying the main EDL behavior [25]. The C_g of GF-SC and NGF-SC are 203 and 225 F g^{-1}, respectively. The higher C_g of NGF-SC also results from more pseudocapacitance stemmed from active nitrogen sites. After grafting with PANi, the curve of the PNGF shows two different parts: 0.8–0.45 V, corresponding to EDL capacitance; 0.45–0 V, corresponding to the combination of EDL and Faradic capacitances of PANi-graphene component [24]. Benefiting from the better doping of PANi on the precursor of NGF, the C_g of the PNGF-SC can reach 360 F g^{-1}, which is much higher than that of the PGF-SC (289 F g^{-1}). Compared with other GP materials, our PNGF-SC exhibits high electrochemical performance (Table S2) [23,24,26–33]. Both the PNGF-SC and PGF-SC have small dynamic voltage drops, which are 0.0031 and 0.0033 V, respectively. Rate capability of PNGF is shown in Fig. 4c. Even at a high current density of 100 A g^{-1} (Fig. S6), PNGF electrode still retains 275 F g^{-1}, indicating 76% retention as the current density increases 100 times. Obviously, the high rate capability of PNGF is also due to the crumpled inner structures inherited from NGF precursor. The PNGF electrodes perform gravimetric energy density (E_g) of 8.0 W h kg^{-1} with gravimetric power density (P_g) of 800 W kg^{-1}. Even under high power density (40,000 W kg^{-1}), the E_g still retains 7.3 W h kg^{-1} (Fig. S7).

EIS was employed to analyze the resistance behaviors of electrodes. The low-frequency portions of the Nyquist plots of all the supercapacitors are nearly vertical to the axis at low frequencies, which implies an ideal capacitive behavior (Fig. 4d) [34]. Equivalent series resistance (R_{ESR}) is mainly composed of three parts: 1) the intrinsic ohmic resistance R_s (the first intercept along the real axis), 2) the interfacial charge transfer resistance R_{ct} (the diameter of the semicircle), and 3) Warburg diffusion resistance R_w [18]. By extrapolating the portion of the low frequency to the real axis, the R_{ESR} was obtained for the GF-SC (11.84 ohm), PGF-SC (3.34 ohm), NGF-SC (5.20 ohm) and PNGF-SC (2.12 ohm), respectively. The precursor NGF has a much smaller R_{ESR} than GF, and the trend is retained after drafting with PANi. Since all of the four films have similar R_s, the differences between the two precursors and between their subsequent products are mostly contributed by R_{ct} and R_w (Table S3). As wettability between the electrolyte and electrode is one of the decisive factors of R_{ct} and R_w [35–38], the hydrophilic NGF precursor contributes greatly to the connection between its subsequent product PNGF and the electrolyte. GF and its subsequent product PGF show poor resistance behavior, which is also proved by the dynamic contact angle measurements in Fig. 3.

The cycling performance of the PNGF-SC was tested by GCD at 2 A g^{-1} for 20,000 cycles. As shown in Fig. 4e, the PNGF-SC achieves an extremely high cycling stability (78% retention after cycling) at the top level in GP-SC

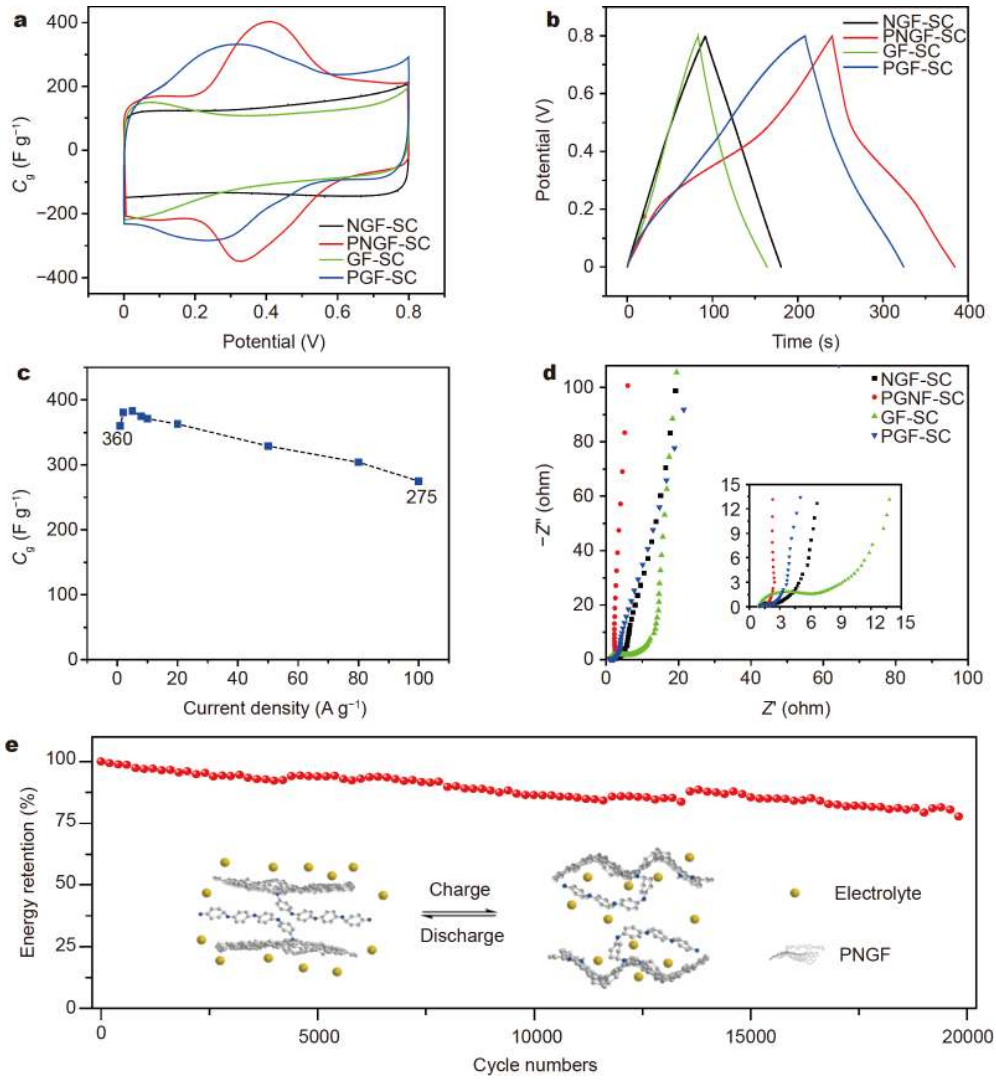

Figure 4 Electrochemical performance of NGF-SC, PNGF-SC, GF-SC and PGF-SC. (a) CV curves of NGF-SC, PNGF-SCy, GF-SC and PGF-SC measured at a scan rate of 10 mV s^{-1}. (b) GCD curves of NGF-SC, PNGF-SC, GF-SC and PGF-SC measured at a current density of 1 A g^{-1}. (c) Rate capability of PNGF-SC calculated by GCD curves from 1 to 100 A g^{-1}. (d) Nyquist plots of NGF-SC, PNGF-SC, GF-SC and PGF-SC with the equivalent circuit. The inset shows the magnified high-frequency region. (e) Cycling stability of PNGF-SC at 2 A g^{-1}. The inset shows the schematic of proposed charge-discharge mechanism of PNGF-SC.

systems [12,17,19,24,39]. The inset in Fig. 4e shows the proposed charge-discharge mechanism of PNGF-SC. The improved cycling stability of the PNGF-SC may be ascribed to the grafting combining mode between the NGF and PANi. Such combination prevents the composite from severely swelling and shrinking of the polymer skeleton induced by the movement of ions [40]. Hence, the morphological and electrochemical property of PNGF during charging and discharging cycling are maintained. Therefore, the as-prepared PNGF-SC exhibits excellent cycling stability.

The effect of the bending-induced mechanical stress on the electrochemical performance of the PNGF was investigated. PNGF displays almost the same charge-discharge behavior at different bending states (Fig. S8). The capacitance (360 F g^{-1}) still retains 78% after 1,000 bending cycles (Fig. S9), revealing the great flexibility and stability of the PNGF based supercapacitor.

In view of the commercial requirements, the mass loading of SC electrodes should be higher than 10 mg cm^{-2} to achieve demanded energy density [41]. However, GP electrodes suffer from low mass loading [42,43], due to the unsatisfactory inner structure and unsuitable material design. By simply changing the out-

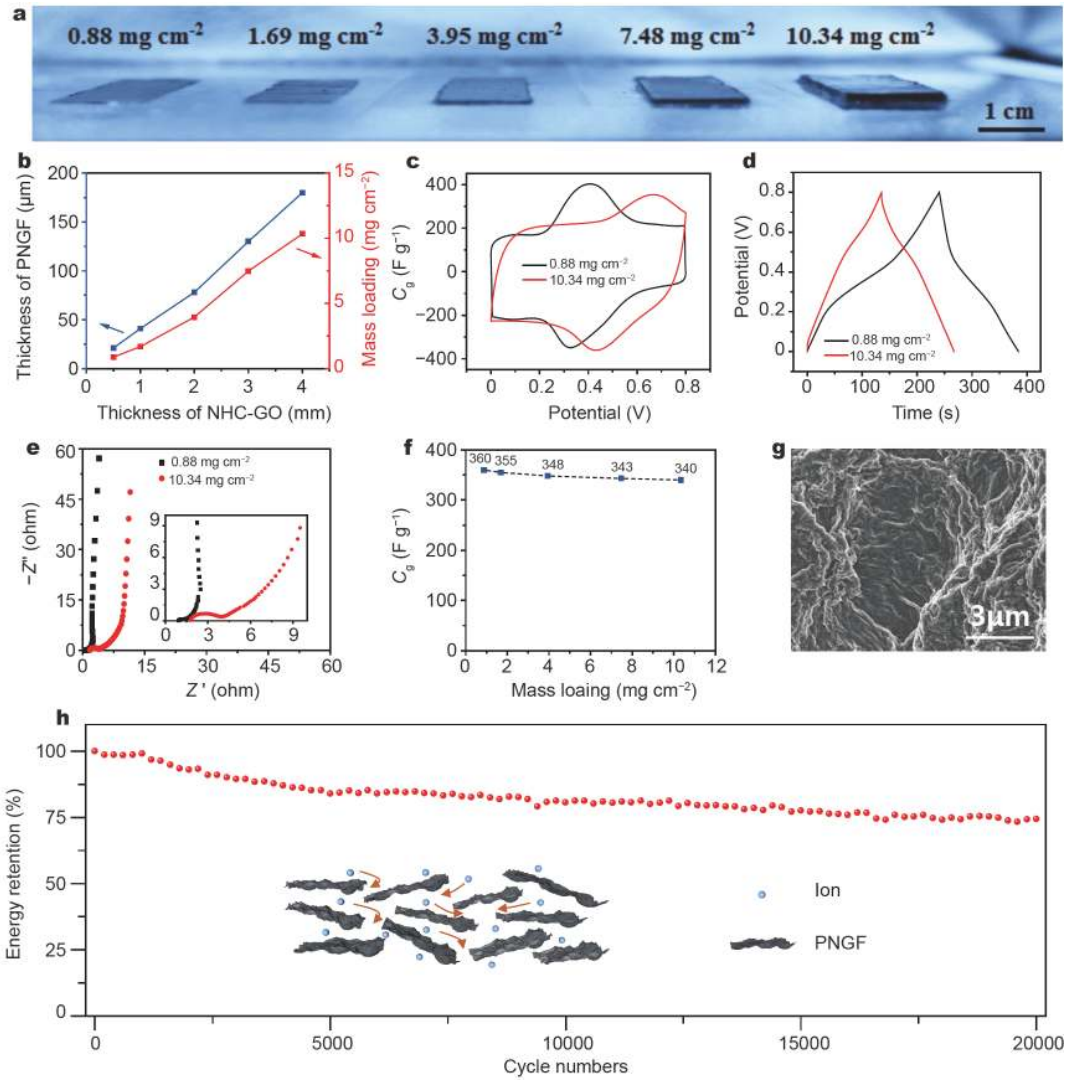

Figure 5 (a) Photograph of NGF hydrogels with different thicknesses. (b) Mass loading of the PNGF is nearly proportional to the thickness of its precursor NGF hydrogel. (c) CV curves of $PNGF_{0.88}$-SC and $PNGF_{10.34}$-SC at the scan rate of 10 mV s^{-1}. (d) The GCD curves of $PNGF_{0.88}$-SC and $PNGF_{10.34}$-SC under the current density of 1 A g^{-1}. (e) Nyquist plots of $PNGF_{0.88}$-SC and $PNGF_{10.34}$-SC with the equivalent circuit. The inset shows the magnified high-frequency region. (f) Effects of mass loading on C_g of PNGF-SC. (g) Top-view SEM image of the surface of PNGF. (h) Cycling stability of $PNGF_{10.34}$-SC at 2 A g^{-1}. The inset is the schematic illustration of ion transport in $PNGF_{10.34}$-SC.

put thickness of nozzle, we can fabricate NGF hydrogels with different thicknesses and thus different mass loadings of the final NGF electrodes (Fig. 5a). Furthermore, PNGF with different levels of mass loading was obtained using NGF precursors with different thicknesses. Fig. 5b illustrates nearly a proportional linear relationship between the thickness of NGF hydrogels and the mass loading of final PNGF, reflecting the controllability of wet-spinning technology.

The relationship between mass loading and electrochemical performance of PNGF based electrodes was studied. The CV curves in Fig. 5c exhibit two obvious peaks under low mass loading (0.88 mg cm^{-2}) or high mass loading (10.34 mg cm^{-2}), indicating the maintained redox reaction of PANi during charge and discharge regardless of mass loading. The shift of redox peaks under high voltage with high mass loading is due to the increased resistance, proved by EIS in Fig. 5e. Both the GCD curves of $PNGF_{0.88}$-SC and $PNGF_{10.34}$-SC at 1 A g^{-1} exhibit two pseudocapacitor stages (Fig. 5d), indicating the good performance delivery from crumpled structures. The C_gs of the assembled PNGF-SCs with different mass loadings are shown in Fig. 5f. As the mass loading increases from 0.88 to 10.34 mg cm^{-2}, the C_g decreases

slowly from 360 to 340 F g^{-1}, with 94% retention. Compared with the rate performance of other high mass loading G-PANi, our PNGF is at the top class with high specific capacitance [14,23,44]. This benefits from the excellent ion transportation efficiency through the carbon skeleton, inherited from the precursor NGF [10]. Even at a high current density of 10 A g^{-1} (Fig. S11), $PNGF_{10.34}$ electrode still retains 237 F g^{-1}, demonstrating its high rate capability under high mass loading. The SEM image shown in Fig. 5g indicates large holes on the surface of the PNGF, resulting in channels for ions permeating deeply into the films, which can additionally explain the good performance of $PNGF_{10.34}$. Even with high mass loading, $PNGF_{10.34}$ still exhibits excellent cycling stability (74% retention after 20,000 cycles, 2 A g^{-1}) (Fig. 5h), which can be ascribed to the grafting combining mode and the well-designed inner structure, as shown in the inset of Fig. 5h. Due to the wettable interface and expanded interlayer of PNGF, the electrolyte ions from the solution could rapidly attach on the surface of electrodes and penetrate efficiently across the crumpled sheets. With this unique structure, PNGF with high mass loading possesses a long lifespan, which is of great significance for practical SCs.

CONCLUSIONS

In summary, we have fabricated a kind of wettable PNGF free-standing electrode *via* wet-spinning with outstanding SC behavior. The properties of PNGF are mainly inherited from the NGF precursor. The nitrogen atoms doped on the graphene sheets not only provides the original grafting sites of aniline but also improves the wettability, resulting in stable and considerable growth of PANi. Even under high mass loading, the as-prepared PNGF maintains good electrochemical performance with long cycling stability, due to the delicate design of the surface and inner structure. This work sheds a light on the practical applications of GP-electrodes.

Received 26 February 2019; accepted 7 May 2019; published online 22 May 2019

1 Liu C, Li F, Ma LP, *et al.* Advanced materials for energy storage. Adv Mater, 2010, 22: E28–E62
2 Zhu Y, Murali S, Cai W, *et al.* Graphene and graphene oxide: Synthesis, properties, and applications. Adv Mater, 2010, 22: 3906–3924
3 Frackowiak E, Béguin F. Carbon materials for the electrochemical storage of energy in capacitors. Carbon, 2001, 39: 937–950
4 Du Pasquier A, Laforgue A, Simon P, *et al.* A nonaqueous asymmetric hybrid $Li_4Ti_5O_{12}$/poly(fluorophenylthiophene) energy storage device. J Electrochem Soc, 2002, 149: A302
5 Talbi H, Just PE, Dao LH. Electropolymerization of aniline on carbonized polyacrylonitrile aerogel electrodes: Applications for supercapacitors. J Appl Electrochem, 2003, 33: 465–473
6 Snook GA, Kao P, Best AS. Conducting-polymer-based supercapacitor devices and electrodes. J Power Sources, 2011, 196: 1–12
7 Liu Z, Li Z, Xu Z, *et al.* Wet-spun continuous graphene films. Chem Mater, 2014, 26: 6786–6795
8 Xu Z, Gao C. Graphene in macroscopic order: Liquid crystals and wet-spun fibers. Acc Chem Res, 2014, 47: 1267–1276
9 Xu Z, Gao C. Aqueous liquid crystals of graphene oxide. ACS Nano, 2011, 5: 2908–2915
10 Huang T, Chu X, Cai S, *et al.* Tri-high designed graphene electrodes for long cycle-life supercapacitors with high mass loading. Energy Storage Mater, 2019, 17: 349–357
11 Kudin KN, Ozbas B, Schniepp HC, *et al.* Raman spectra of graphite oxide and functionalized graphene sheets. Nano Lett, 2008, 8: 36–41
12 Cong HP, Ren XC, Wang P, *et al.* Flexible graphene–polyaniline composite paper for high-performance supercapacitor. Energy Environ Sci, 2013, 6: 1185
13 Huang T, Zheng B, Liu Z, *et al.* High rate capability supercapacitors assembled from wet-spun graphene films with a $CaCO_3$ template. J Mater Chem A, 2015, 3: 1890–1895
14 Yan J, Wei T, Fan Z, *et al.* Preparation of graphene nanosheet/carbon nanotube/polyaniline composite as electrode material for supercapacitors. J Power Sources, 2010, 195: 3041–3045
15 Zou Y, Zhang Z, Zhong W, *et al.* Hydrothermal direct synthesis of polyaniline, graphene/polyaniline and n-doped graphene/polyaniline hydrogels for high performance flexible supercapacitors. J Mater Chem A, 2018, 6: 9245–9256
16 Xu Y, Tao Y, Zheng X, *et al.* A metal-free supercapacitor electrode material with a record high volumetric capacitance over 800 F cm^{-3}. Adv Mater, 2015, 27: 8082–8087
17 Wang H, Hao Q, Yang X, *et al.* A nanostructured graphene/polyaniline hybrid material for supercapacitors. Nanoscale, 2010, 2: 2164–2170
18 Zhao J, Jiang Y, Fan H, *et al.* Porous 3D few-layer graphene-like carbon for ultrahigh-power supercapacitors with well-defined structure-performance relationship. Adv Mater, 2017, 29: 1604569
19 Wang H, Hao Q, Yang X, *et al.* Effect of graphene oxide on the properties of its composite with polyaniline. ACS Appl Mater Interfaces, 2010, 2: 821–828
20 Chen LF, Zhang XD, Liang HW, *et al.* Synthesis of nitrogen-doped porous carbon nanofibers as an efficient electrode material for supercapacitors. ACS Nano, 2012, 6: 7092–7102
21 Alhabeb M, Beidaghi M, Van Aken KL, *et al.* High-density free-standing graphene/carbide-derived carbon film electrodes for electrochemical capacitors. Carbon, 2017, 118: 642–649
22 Khomenko V, Frackowiak E, Béguin F. Determination of the specific capacitance of conducting polymer/nanotubes composite electrodes using different cell configurations. Electrochim Acta, 2005, 50: 2499–2506
23 Mishra AK, Ramaprabhu S. Functionalized graphene-based nanocomposites for supercapacitor application. J Phys Chem C, 2011, 115: 14006–14013
24 Wu Q, Xu Y, Yao Z, *et al.* Supercapacitors based on flexible graphene/polyaniline nanofiber composite films. ACS Nano, 2010, 4: 1963–1970
25 Li R, Ren X, Zhang F, *et al.* Synthesis of Fe_3O_4@SnO_2 core–shell nanorod film and its application as a thin-film supercapacitor

electrode. Chem Commun, 2012, 48: 5010–5012
26 Li L, Raji ARO, Fei H, *et al.* Nanocomposite of polyaniline nanorods grown on graphene nanoribbons for highly capacitive pseudocapacitors. ACS Appl Mater Interfaces, 2013, 5: 6622–6627
27 Li ZF, Zhang H, Liu Q, *et al.* Fabrication of high-surface-area graphene/polyaniline nanocomposites and their application in supercapacitors. ACS Appl Mater Interfaces, 2013, 5: 2685–2691
28 Xu Y, Schwab MG, Strudwick AJ, *et al.* Screen-printable thin film supercapacitor device utilizing graphene/polyaniline inks. Adv Energy Mater, 2013, 3: 1035–1040
29 Hao Q, Xia X, Lei W, *et al.* Facile synthesis of sandwich-like polyaniline/boron-doped graphene nano hybrid for supercapacitors. Carbon, 2015, 81: 552–563
30 Lee T, Yun T, Park B, *et al.* Hybrid multilayer thin film supercapacitor of graphene nanosheets with polyaniline: Importance of establishing intimate electronic contact through nanoscale blending. J Mater Chem, 2012, 22: 21092–21099
31 Xie Y, Liu Y, Zhao Y, *et al.* Stretchable all-solid-state supercapacitor with wavy shaped polyaniline/graphene electrode. J Mater Chem A, 2014, 2: 9142–9149
32 Zhang J, Zhao XS. Conducting polymers directly coated on reduced graphene oxide sheets as high-performance supercapacitor electrodes. J Phys Chem C, 2012, 116: 5420–5426
33 Dong X, Wang J, Wang J, *et al.* Supercapacitor electrode based on three-dimensional graphene–polyaniline hybrid. Mater Chem Phys, 2012, 134: 576–580
34 Hsia B, Marschewski J, Wang S, *et al.* Highly flexible, all solid-state micro-supercapacitors from vertically aligned carbon nanotubes. Nanotechnology, 2014, 25: 055401
35 Li X, Rong J, Wei B. Electrochemical behavior of single-walled carbon nanotube supercapacitors under compressive stress. ACS Nano, 2010, 4: 6039–6049
36 Luo J, Jang HD, Huang J. Effect of sheet morphology on the scalability of graphene-based ultracapacitors. ACS Nano, 2013, 7: 1464–1471
37 Bo Z, Zhu W, Ma W, *et al.* Vertically oriented graphene bridging active-layer/current-collector interface for ultrahigh rate supercapacitors. Adv Mater, 2013, 25: 5799–5806
38 Zhao J, Lai H, Lyu Z, *et al.* Hydrophilic hierarchical nitrogen-doped carbon nanocages for ultrahigh supercapacitive performance. Adv Mater, 2015, 27: 3541–3545
39 Zhang K, Zhang LL, Zhao XS, *et al.* Graphene/polyaniline nanofiber composites as supercapacitor electrodes. Chem Mater, 2010, 22: 1392–1401
40 Sun Y, Shi G. Graphene/polymer composites for energy applications. J Polym Sci B Polym Phys, 2013, 51: 231–253
41 Tang C, Yin X, Gong H. Superior performance asymmetric supercapacitors based on a directly grown commercial mass 3D Co_3O_4@Ni(OH)$_2$ core–shell electrode. ACS Appl Mater Interfaces, 2013, 5: 10574–10582
42 Yu S, Wang X, Ai Y, *et al.* Experimental and theoretical studies on competitive adsorption of aromatic compounds on reduced graphene oxides. J Mater Chem A, 2016, 4: 5654–5662
43 He Y, Chen W, Li X, *et al.* Freestanding three-dimensional graphene/MnO_2 composite networks as ultralight and flexible supercapacitor electrodes. ACS Nano, 2013, 7: 174–182
44 Ates M, El-Kady M, Kaner RB. Three-dimensional design and fabrication of reduced graphene oxide/polyaniline composite hydrogel electrodes for high performance electrochemical supercapacitors. Nanotechnology, 2018, 29: 175402

Acknowledgements This work is supported by the National Natural Science Foundation of China (51533008, 21325417, 51603183, 51703194, 51803177 and 21805242), the National Key R&D Program of China (2016YFA0200200), Fujian Provincial Science and Technology Major Projects (2018HZ0001-2), Hundred Talents Program of Zhejiang University (188020*194231701/113), the Key Research and Development Plan of Zhejiang Province (2018C01049), and the Fundamental Research Funds for the Central Universities (2017QNA4036 and 2017XZZX001-04).

Author contributions Chu X and Huang T designed the strategy. Chu X, Hu Y, Dong R and Luo J performed the experiments. Chu X wrote the paper with support from Huang T, Cai S, Gao W, Xu Z and Gao C. All authors contributed to the general discussion.

Conflict of interest The authors declare no conflict of interest.

Supplementary information Supporting data are available in the online version of the paper.

Tieqi Huang graduated from Shanghai Jiao Tong University (SJTU) in 2011 and obtained his PhD degree from Zhejiang University in 2018. Currently he is doing postdoctoral research at Nanjing Tech University. His research interests focus on the energy storage, especially supercapacitor.

Chao Gao obtained his PhD degree from Shanghai Jiao Tong University (SJTU) in 2001. He was appointed as an Associate Professor at SJTU in 2002. He did postdoctoral research at the University of Sussex with Prof. Sir Harry W. Kroto and AvH research at Bayreuth University with Prof. Axel H. E. Muller during 2003–2006. He joined the Department of Polymer Science and Engineering, Zhejiang University in 2008 and was promoted as a full Professor. His research interests focus on graphene chemistry, macroscopic assembly, and energy storage.

湿纺组装氮掺杂石墨烯薄膜用于高稳定性石墨烯-聚苯胺超级电容器电极

褚星远, 黄铁骑*, 胡玥琪, 董瑞临, 骆靖阳, 蔡盛赢, 高微微, 许震, 高超*

摘要 石墨烯-聚苯胺(GP)复合材料是一种有前途的超级电容器电极材料, 但其稳定性较差, 尤其在负载量高的情况下. 低离子传输效率和严重的粉碎效应是导致这一结果的主要原因. 为了解决这个问题, 我们提出了一种可规模化制备高度可润湿GP电极的方法, 该电极显示出优异的稳定性. 此外, 研究结果表明电极的性能几乎与负载量无关, 因此这种GP电极在实际生产中具有巨大潜力. 通过湿纺技术组装的氮掺杂石墨烯薄膜前驱体使得这种电极材料表现出卓越性能. 这种提高电极间离子渗透效率并阻止粉碎效应的方法, 旨在制备实用型高负载量的GP超级电容器电极.

